Amine-Terminated Silver Nanoparticles Exhibit Potential for Selective Targeting of Triple-Negative Breast Cancer

Jayshree H. Ahire [1,*], Qi Wang [2], Yuewei Tao [3], Yimin Chao [1] and Yongping Bao [2]

1 School of Chemistry, University of East Anglia, Norwich NR4 7TJ, UK; y.chao@uea.ac.uk
2 Norwich Medical School, University of East Anglia, Norwich NR4 7TJ, UK; q.wang1@uea.ac.uk (Q.W.); y.bao@uea.ac.uk (Y.B.)
3 School of Medicine, University of Dundee, Dundee DD2 1UU, UK; 2406970@dundee.ac.uk
* Correspondence: j.ahire@uea.ac.uk

Abstract: Silver nanoparticles (AgNPs) demonstrate potential in treating aggressive cancers such as triple-negative breast cancer (TNBC) in preclinical models. To further the development of AgNP-based therapeutics for clinical use, it is essential to clearly define the specific physicochemical characteristics of the nanoparticles and connect these properties to biological outcomes. This study addresses this knowledge gap through detailed investigations into the structural and surface functional relationships, exploring the mechanisms, safety, and efficacy of AgNPs in targeting TNBC. The surface functionality of nanoparticles is crucial not only for their internalization into cancer cells but also for enhancing their toxicity toward tumor cells. Although the nanoparticles internalized into cancer cells, they failed to exhibit their full toxicity against the cancer. Herein we report a solvent-assisted synthesis amine, mercaptohexanol and bifunctional silver nanoparticles and performing comparative study to understand their selectivity and toxicity toward TNBC cells. The nanoparticles are fully characterized by UV–visible absorption spectroscopy, Fourier transform infrared spectroscopy (FTIR), scanning electron microscopy (SEM), and dynamic light scattering measurement (DLS). The synthesis method achieves an extremely high yield and surface coating ratio of synthesized colloidal AgNPs. Our findings reveal that the amine-capped AgNPs exhibit significant selective toxicity against TNBC cell lines MCF7 and MDA-MB-231 at a concentration of 40 μg/mL without affecting normal breast cell lines MCF10A. This study underscores the potential of functionalized AgNPs in developing safe and targeted therapeutic approaches for treating aggressive cancers like TNBC, laying the groundwork for future clinical advancements.

Keywords: triple-negative breast cancer; silver nanoparticles; cysteamine; mercaptohexanol; selective targeting; toxicity

1. Introduction

Triple-negative breast cancer (TNBC) presents unique treatment challenges due to its lack of hormone and HER2 receptors, excluding patients from receptor-targeted therapies like those used in other breast cancer subtypes [1,2]. TNBC is highly metastatic, more aggressive, and biologically diverse, resulting in a higher relapse rate and poorer prognosis [3]. Standard treatments, including surgery, radiation, and chemotherapy, are limited by their invasiveness and severe side effects. Chemotherapy drugs such as taxanes, though widely used, pose risks of dose-limiting toxicities and secondary cancers, offering limited specificity for TNBC cells [4,5]. As a result, there is a critical need for the development of novel, targeted therapeutic approaches that address the heterogeneity and aggressiveness of TNBC, while minimizing off-target effects. Advances in precision medicine, immunotherapy, and nanoparticle-based delivery systems hold promise for future breakthroughs in TNBC treatment, potentially improving both patient outcomes and quality of life.

Several studies have focused on using nanoparticles as drug carriers, aiming to improve bioavailability and targeted delivery of therapeutic agents to tumors. However, a

significant challenge remains in their poor tumor-targeting abilities, which leads to concerns over off-target toxicity [6,7]. While nanoparticles made from metals like gold, silver, iron, and gadolinium have demonstrated anticancer potential by exploiting cancer-specific vulnerabilities, silver nanoparticles (AgNPs) are of particular interest [8–12]. Gold nanoparticles are well-regarded for their ease of functionalization and effectiveness in imaging and photothermal therapy, but they can be expensive and may pose toxicity risks at high concentrations [13]. Magnetic nanoparticles, like iron oxide, are utilized for targeted drug delivery and magnetic resonance imaging; however, they can exhibit toxicity, and their magnetic properties may complicate certain imaging techniques [14,15]. Apart from that, quantum dots are highly effective for fluorescence imaging due to their unique optical properties, but they often contain toxic heavy metals and can suffer from photobleaching [16,17]. Carbon dots, a newer class of nanoparticles, are gaining attention in 3D tumor models due to their biocompatibility, low toxicity, and optical properties, making them suitable for bioimaging and drug delivery [18,19]. However, they face challenges in synthesis consistency, potential photobleaching, and less efficient targeting compared to other nanoparticles. Additionally, concerns regarding their long-term biocompatibility and regulatory hurdles may hinder their clinical use. In comparison, AgNPs are less expensive and possess strong antimicrobial properties, which can be beneficial in therapeutic settings [20–22].

Silver nanoparticles are gaining increasing attention in cancer research, due to their intriguing physical–chemical features, showing inherent antiproliferative action. Their strong antimicrobial properties have long been recognized, but recent studies have also uncovered their cytotoxic effects against a wide variety of cancers, including breast [23], ovarian [24], brain [25–27], cervical [28], liver [29], and others [30–35]. AgNPs have shown promise in selectively targeting cancer cells without causing significant damage to surrounding healthy tissues.

Despite limited clinical trials, there are intriguing case reports, such as one involving the complete regression of metastatic head and neck cancer after a patient ingested AgNPs, following the failure of conventional treatments [36]. This underscores the potential of AgNPs in cancer therapy. However, as AgNPs are pleiotropic agents, sub-lethal effects need careful examination to ensure their safety in clinical applications.

Silver nanoparticles exhibit broad-spectrum anticancer effects through multiple mechanisms. Research shows that AgNPs can inhibit cancer cell growth and induce cell death by damaging cellular structures, generating reactive oxygen species (ROS), and causing DNA damage. This leads to apoptosis or necrosis. Additionally, AgNPs can provoke endoplasmic reticulum (ER) stress and activate the unfolded protein response (UPR). Prolonged UPR activation may trigger apoptosis, providing a targeted cancer therapy route. By inhibiting tumor cell migration and angiogenesis, AgNPs may also reduce distant metastasis. To develop a safe and effective anticancer drug, further studies are needed to explore additional mechanisms underlying AgNPs' anticancer effects. The physicochemical properties of AgNPs, including size, shape, and surface coating, are crucial for optimizing their cytotoxicity and therapeutic potential. Thus, detailed investigation of these aspects is vital for safe and effective cancer treatment.

In this study, we hypothesize that TNBC cells are particularly vulnerable to AgNP-induced stress and explore how different functionality (cysteamine, mercaptohexanol and bifunctional MH+cyst) on the surface of nanoparticles affects the sensitivity of TNBC cells.

Cysteamine is a small molecule with versatile biomedical applications, including its FDA-approved use in treating cystinosis. It has shown potential in various disease therapies, such as cancer, where it exhibits anticancer properties by inhibiting tumor proliferation, preventing metastasis, and inducing autophagy [37]. Cysteamine's thiol group makes it an excellent candidate for functionalizing nanoparticles, enhancing their stability and therapeutic capabilities. When linked to nanoparticles, it can serve as an efficient drug delivery vector and sensor, yet its combination with silver nanoparticles for cancer therapy is underexplored.

Cysteamine offers the advantage of functioning as a linker between silver nanoparticles and targeting agents. Its surface coating, rich in amino groups, facilitates the controlled attachment of targeting antibodies. This provides the nanoparticle with a stable layer that not only aids in orienting binding sites but also contributes additional antitumor properties. The dual functionality of cysteamine, both in binding and enhancing therapeutic effects, makes it a valuable component in nanoparticle-based drug delivery systems for cancer treatment.

6-mercapto-1-hexanol (MCH), a small molecule with a thiol group, used to prevent nonspecific adsorption on surfaces, such as those used in biosensors. Mercaptohexanol-functionalized silver nanoparticles hold potential in cancer treatment due to their unique properties. Functionalization with MCH enhances nanoparticle stability and reduces nonspecific adsorption, which improves targeting and recognition of cancer cells. Silver nanoparticles are known for their cytotoxic effects, inducing ROS, DNA damage, and cellular stress, ultimately leading to cancer cell death. By functionalizing AgNPs with MCH, it may improve their effectiveness in selectively targeting tumor cells while minimizing unwanted interactions, enhancing their therapeutic potential in cancer treatments. In this study, we employed MCH to investigate the internalization and toxicity of MH-AgNPs in cancer cells, with a focus on TNBC cells. The aim was to understand how surface functionality influences not only the nanoparticles' ability to penetrate cancer cells but also their role in selectively inducing toxicity in these cells.

We used a range of techniques to fully characterize these AgNPs, ensuring precise control over their properties to better understand how such variations influence their biological effects. This research could provide important insights into developing more effective nanoparticle-based therapies for TNBC and other aggressive cancers.

2. Materials and Methods

2.1. Materials

Silver nitrate ($AgNO_3$) and dimethylaminopyridine (DMAP) were purchased from Fisher Scientific, Loughborough, UK. Sodium borohydride ($NaBH_4$), 2-mercaptoethylamine hydrochloride (cysteamine), 6-Mercaptohexanoic acid, 3-(4,5-dimethyl-2-thiazolyl)-2,5-diphenyl tetrazolium bromide (MTT) and dimethylformamide (DMF) were purchased from Sigma-Aldrich, Dorset, UK.

2.2. Synthesis of Amine-Capped Silver Nanoparticles (Cyst-AgNPs)

The amine-terminated silver nanoparticles were synthesized using reduction of silver nitrate in the presence of cysteamine hydrochloride as a stabilizing agent. In a standard reaction setup, 20 mL of DMF was added in an Erlenmeyer flask containing a magnetic stirrer bar. The flask was then placed in an ice bath, and sequentially, aqueous solutions of cysteamine (0.7 mmol, 0.5 mL) and $AgNO_3$ (0.234 mmol, 0.5 mL) were added. The reaction mixture was stirred for 10 min, after which an aqueous solution of $NaBH_4$ (3 mL, 210 mM) was added dropwise. A rapid color change from milky white to yellowish brown was observed. The reaction mixture was stirred for an additional 30 min. The amine-capped silver nanoparticles (Cyst-AgNPs) were collected and purified by centrifugation (8000 rpm, 10 min) after washing three times with DMF. The resulting dark brown pallet of synthesized nanoparticles were re-suspended in water.

2.3. Synthesis of Mercaptohexanol-Capped Silver Nanoparticles (MH-AgNPs)

The mecrcaptohexanol-terminated silver nanoparticles were synthesized using reduction of silver nitrate in the presence of 6-mercaptohexanol as a stabilizing agent. In a standard reaction setup, 20 mL of DMF was added in an Erlenmeyer flask containing a magnetic stirrer bar. The flask was then placed in an ice bath, and sequentially, aqueous solutions of mercaptohexanol (0.7 mmol, 0.5 mL) and $AgNO_3$ (0.234 mmol, 0.5 mL) were added. The reaction mixture was stirred for 10 min, after which an aqueous solution of $NaBH_4$ (3 mL, 210 mM) was added dropwise. A rapid color change from milky white to

yellowish brown was observed. The reaction mixture was immediately precipitated with acetone and the nanoparticles were collected and purified by centrifugation (8000 rpm, 10 min) after washing three times with water. The resulting dark brown pallet of synthesized nanoparticles were re-suspended in water.

2.4. Synthesis of MH-cyst-Capped Silver Nanoparticles (MH+cyst-AgNPs)

The MH+cyst silver nanoparticles were synthesized using reduction of silver nitrate in the presence of 6-mercaptohexanol and cysteamine hydrochloride as a stabilizing agent. In a standard reaction setup, 20 mL of DMF was added in an Erlenmeyer flask containing a magnetic stirrer bar. The flask was then placed in an ice bath, and sequentially, aqueous solutions of mercaptohexanol (0.35 mmol, 0.5 mL), cysteamine hydrochloride (0.35 mmol, 0.5 mL) and $AgNO_3$ (0.234 mmol, 0.5 mL) were added. The reaction mixture was stirred for 10 min, after which an aqueous solution of $NaBH_4$ (3 mL, 210 mM) was added dropwise. A rapid color change from milky white to yellowish brown was observed. The reaction mixture was stirred for an additional 5 min. MH+cyst-AgNPs were precipitated in acetone and purified by centrifugation (8000 rpm, 10 min) after washing three times with water. The resulting dark brown pallet of synthesized nanoparticles were re-suspended in water.

2.5. Characterization of Silver Nanoparticles

The synthesized AgNPs underwent a series of comprehensive characterizations to confirm their structure and functionalization. These analyses included UV–vis absorption spectroscopy, fourier transform infrared (FTIR) spectroscopy, scanning electron microscopy (SEM), energy-dispersive X-ray spectroscopy (EDX) and dynamic light scattering (DLS) measurement.

The UV–vis absorption spectra of AgNPs were recorded by on a PerkinElmer 35 UV–vis double-beam spectrometer, Shelton, CT, USA in a disposable cuvette. FTIR measurements of Cyst-AgNPs were carried out using a PerkinElmer ATR-FTIR spectrometer, Waltham, MA, USA by depositing a solid powder sample on the sample holder. The hydrodynamic diameter of Cyst-AgNPs was determined by DLS measurement with a Zetasizer Nano ZS (Malvern Instruments Ltd., Worcestershire, UK). The SEM and EDX (Oxford Instruments, Wycombe, UK) measurements were carried out using Zeiss Gemini 300 SEM, Oberkochen, Germany. The nanoparticle samples were prepared by dispersing the AgNPs in ethanol and drop-casting onto a carbon-coated copper grid.

2.6. Cell Culture

The cytotoxicity of synthesized AgNPs was evaluated using MCF-10A, MDA-MB-231, and MCF7 cell lines.

The human breast epithelial cell line MCF-10A and the cancer cell lines MCF-7 and MDA-MB-231 were sourced from the American Type Culture Collection (ATCC) (LGC Standards, London, UK). The MCF-10A normal breast cell line was cultured in DMEM/F12 (Gibco, Thermo Fisher Scientific, Paisley, UK) enriched with 5% horse serum (Gibco, Thermo Fisher Scientific, Paisley, UK), hydrocortisone at 0.5 mg/mL, epidermal growth factor (EGF) at 20 ng/mL (Peprotech, London, UK) and insulin at 10 μg/mL (Sigma Aldrich, Gillingham, Kent, UK), maintained at 37 °C with 5% CO_2. In contrast, the MCF-7 and MDA-MB-231 cancer cells were maintained in Dulbecco's Modified Eagle Medium (DMEM) supplemented with 10% fetal bovine serum (FBS), 2 mM glutamine, penicillin (50 U/mL), and streptomycin (50 mg/mL) (Gibco, Thermo Fisher Scientific, Paisley, UK) under a humidified environment at 37 °C with 5% CO_2.

2.7. Evaluation of Cytotoxicity

The cytotoxicity of AgNPs was evaluated using an MTT assay, which assesses mitochondrial dehydrogenase activity as an indicator of cell viability. In this method, a sterile filtered MTT stock solution in phosphate-buffered saline (PBS) at pH 7.4 (5 mg/mL) was added to each well of a 96-well plate, resulting in a final concentration of 0.5 mg/mL. After

2 h of incubation, the unreacted dye was removed, and the insoluble formazan crystals were dissolved in 100 μL of DMSO. The absorbance was measured at 540 nm with a reference wavelength of 630 nm using a microplate reader (BMG Labtech Ltd., Aylesbury, UK). Cell viability (%) was calculated using the following formula:

$$\text{Cell viability (\%)} = \text{ODtest}/\text{ODcontrol} \times 100\%$$

3. Results

3.1. Synthesis and Characterization of Silver Nanoparticles

Cyst-AgNPs were formulated from the reduction of silver nitrate using sodium borohydride as a reducing agent and cysteamine, as a capping agent depicted in Scheme 1. The reaction was performed in DMF instead of water. Oliva et al. [38] provided a clear explanation for the preference of DMF over water. In their study they emphasize that the synthesis of nanoparticles was effective in DMF but not in water due to the distinct properties of the ligand (cysteamine) and the solvent. The preference for DMF stems from its polar aprotic characteristics, which effectively stabilize the positively charged amine group of cysteamine hydrochloride. In water, cysteamine exhibits a higher propensity for interaction with the nanoparticle surface through both its thiol and amine groups, potentially leading to decreased stability and coating efficiency. By utilizing DMF, they promote the binding of cysteamine predominantly through its thiol group, enhancing the stabilization of the AgNPs.
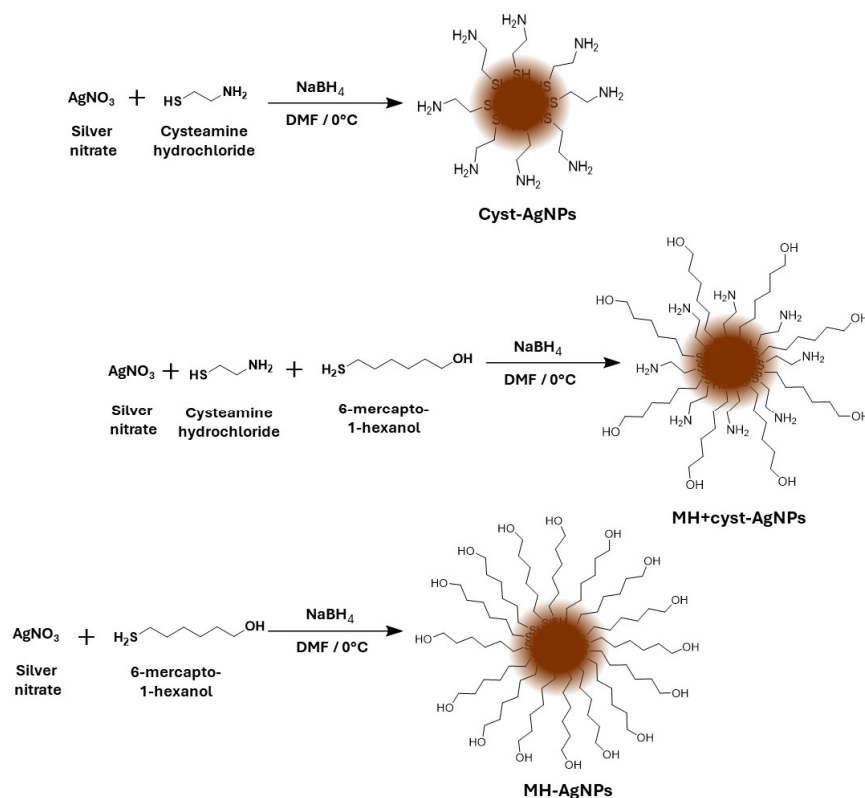
Scheme 1. Schematic representation of synthesis of Cyst-AgNPs, MH+cyst-AgNPs and MH-AgNPs.

The one-pot synthesis method used in the study offers significant advantages over ligand exchange or post-synthesis ligand addition. The presence of a reducing agent in the reaction medium prevents the formation of disulfide bridges, which can occur under atmospheric conditions. This eliminates the need for nanoparticle functionalization under an inert atmosphere, simplifying the process.

The reaction was conducted under carefully controlled conditions to optimize the characteristics of the nanoparticles. For the synthesis of MH-AgNPs and MH+cyst-AgNPs, we followed a similar method and reaction time as outlined by Oliva et al. However, it was observed that extending the reaction time beyond 10 min resulted in the formation of unstable nanoparticles, which precipitated as a black, insoluble mass immediately after halting the reaction. Throughout our investigations, we noted that reaction times ranging from 5 to 20 min affected nanoparticle size, with times exceeding 10 min yielding larger AgNPs that adversely impacted solubility and stability. Consequently, we established a reaction time of 10 min for the synthesis of MH-AgNPs and MH+cyst-AgNPs.

Upon completion of the reaction, the mixture was subjected to immediate centrifugation to halt further synthesis. However, freshly synthesized MH-AgNPs proved challenging to precipitate via centrifugation. To enhance purification, we first precipitated the nanoparticles using acetone before centrifugation, which facilitated efficient recovery. Following centrifugation, the synthesized AgNPs were redispersed in water for subsequent characterization.

Each synthesis batch yielded approximately 20 to 24 mg of nanoparticles. Characterization revealed that each nanoparticle possesses around 30 available binding sites for potential functionalization or interaction with biomolecules, as reported by Oliva et al. [38]. This high degree of functionalization potential underscores the versatility of the synthesized AgNPs for various applications.

The synthesis of Cyst-AgNPs, MH-AgNPs, and MH+cyst-AgNPs demonstrated a delicate balance between reaction time and conditions, with the choice of DMF as a solvent proving critical for achieving optimal nanoparticle stability and functionalization.

3.2. UV–Visible Spectroscopy

The obtained nanoparticles were characterized by UV–vis spectroscopy (Figure 1). The strong absorbance at 400 nm to 550 nm is the characteristic of surface plasmon resonance (SPR) of silver. The absorbance for Cyst-AgNPs has appeared at 450 nm; however, in the case of MH-AgNPs, the absorbance is showing at 500 nm. The results indicate that the change in functionality and possibly the increase in the carbon chain causes the SPR absorbance shift to a higher wavelength. Interestingly, the combination of both capping agents, (MH+cyst-AgNPs) which showed absorbance at 475 nm, exactly at the center of Cyst and MH-AgNPs, proves that the AgNPs is functionalized with MH and Cyst capping ligands.
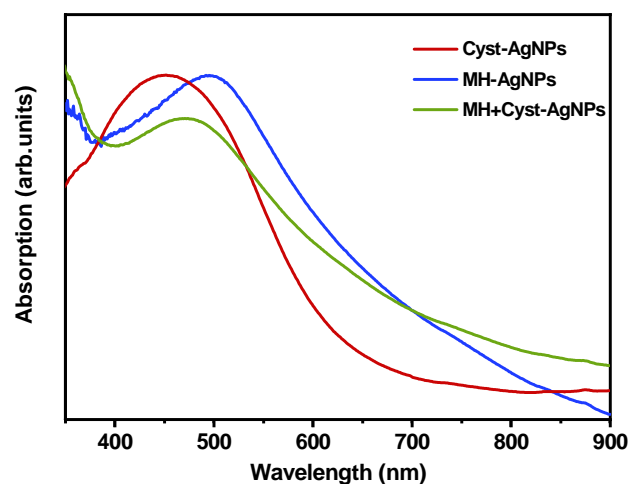
Figure 1. The UV–vis spectra displayed above provide insights into the optical properties of Cyst-AgNPs (red), MH-AgNPs (blue), and MH+cyst-AgNPs (green) when suspended in water. These spectra are instrumental in understanding the formation and stability of the nanoparticles, as well as their surface plasmon resonance (SPR) characteristics.

3.3. FTIR Spectroscopy

The surface functionality of AgNPs was confirmed by FTIR spectroscopy, as shown in Figure 2. The FTIR spectra of MH-AgNPs depicted in Figure 2a were compared with those of 6-mercaptohexanol. Similarly, Figure 2b shows the FTIR spectra of Cyst-AgNPs compared with cysteamine hydrochloride, while Figure 2c presents the FTIR spectra of MH+cyst-AgNPs compared with both mercaptohexanol and cysteamine. The FTIR spectra showed no free SH vibration at 2550–2596 cm^{-1} (highlighted in Figure 2a–c) in all the functionalized AgNPs, demonstrating that the thiol group successfully binds to the surface of the silver nanoparticles.

For MH-AgNPs (Figure 2a), a broad peak at 3400 cm^{-1} was observed, attributed to the stretching vibration of the −OH functionality present in mercaptohexanol. The aliphatic C-H stretching vibrations appeared at 2925 cm^{-1} and 2856 cm^{-1}. In Figure 2b, the broad absorption at 3356 cm^{-1} was attributed to the amine (−NH$_2$) functionality on Cyst-AgNPs, along with a bending vibration at 1580 cm^{-1}. The FTIR spectra of bifunctional MH+cyst-AgNPs demonstrated the dual surface functionalization of both cysteamine and mercaptohexanol, as shown in Figure 2c. The disappearance of the −SH functionality at 2550–2596 cm^{-1} clearly evidenced the surface functionalization of MH+cyst-AgNPs.
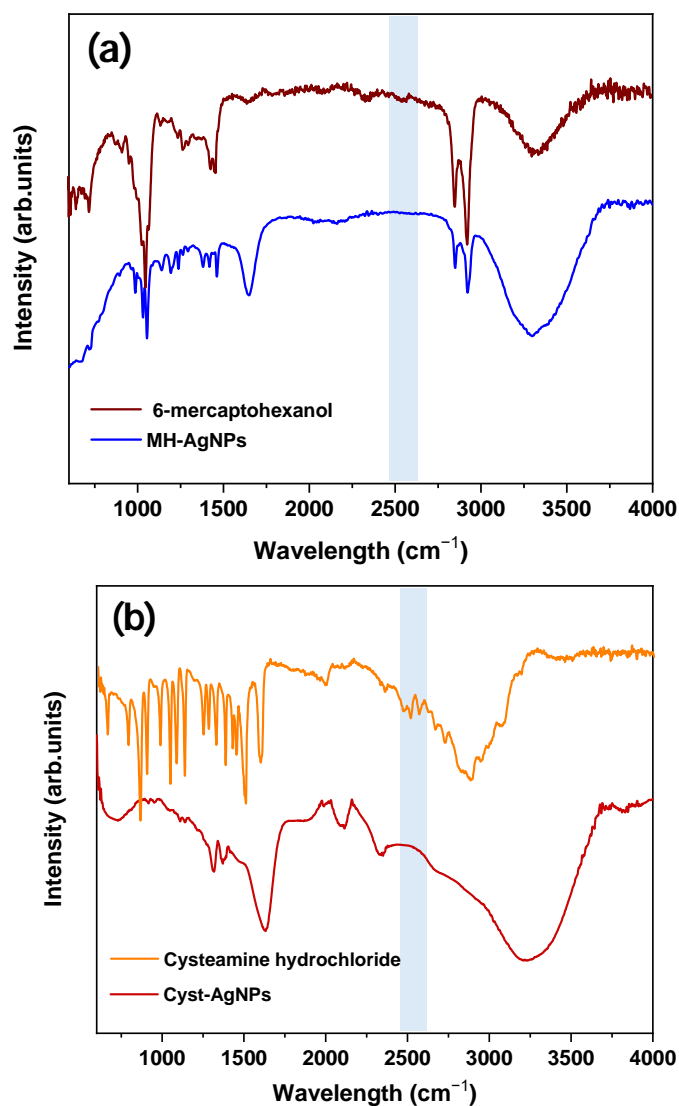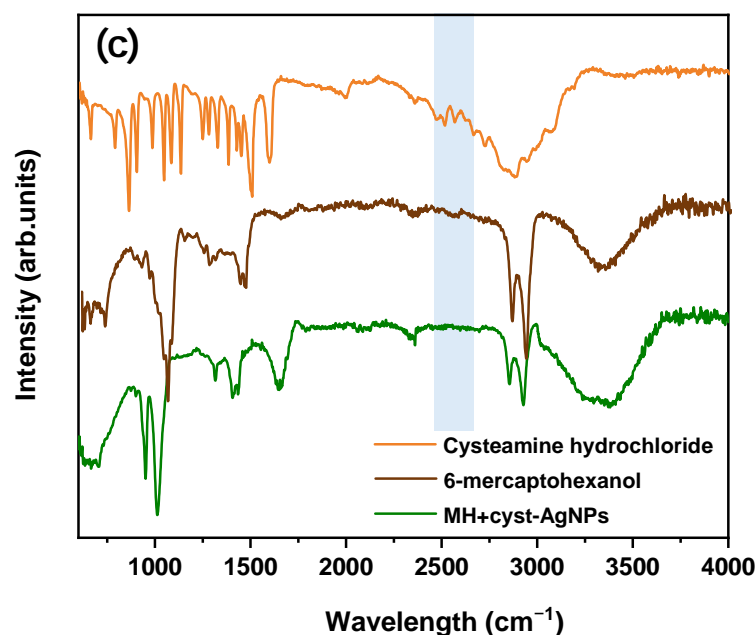

Figure 2. *Cont.*

Figure 2. The Fourier transform infrared (FTIR) spectra presented above illustrate the functional groups and molecular interactions associated with (**a**) Cyst-AgNPs, (**b**) MH-AgNPs, and (**c**) MH+cyst-AgNPs. The ATR spectra of purified solid samples showing the comparison of functionalized silver nanoparticles with their respective capping agents: cysteamine hydrochloride, mercapto hexanol and combination of both. The spectra were normalized with respect to the 1589 cm^{-1} peak. The blue columns indicate the region corresponding to thiol functionality.

The presence of the symmetric and antisymmetric C−H stretching modes indicates the presence of alkyl chains in MH+cyst-AgNPs. The stretching vibration around 3473 cm^{-1} is attributed to the −OH functionality, while the region (3300–3500 cm^{-1}) contains significant contributions from the −NH$_2$ stretching vibrations of cysteamine. The spectrum also contains characteristic peaks of alkyl stretching vibrations between 2800 and 3000 cm^{-1} and the C−O−H bending vibration around 1640 cm^{-1}. Overall, the FTIR spectra confirm the successful surface functionalization of bifunctional MH+cyst-AgNPs.

3.4. Morphological Analysis by SEM Spectroscopy

The SEM analysis presented in Figure 3 provides valuable insights into the morphology of the silver nanoparticles (AgNPs). The images clearly demonstrate the presence of monodisperse particles, which indicates a uniform size distribution throughout the sample. Most notably, the nanoparticles exhibit a predominantly spherical shape, a characteristic that is often associated with enhanced stability and favorable optical properties.

Quantitative analysis reveals that the average diameter of these particles falls within the range of approximately 2–6 nm. This finding aligns well with the dynamic light scattering (DLS) data, which further supports the consistency of the particle size measurements. The agreement between the SEM and DLS results reinforces the reliability of the synthesis process and the effectiveness of the capping agents used.
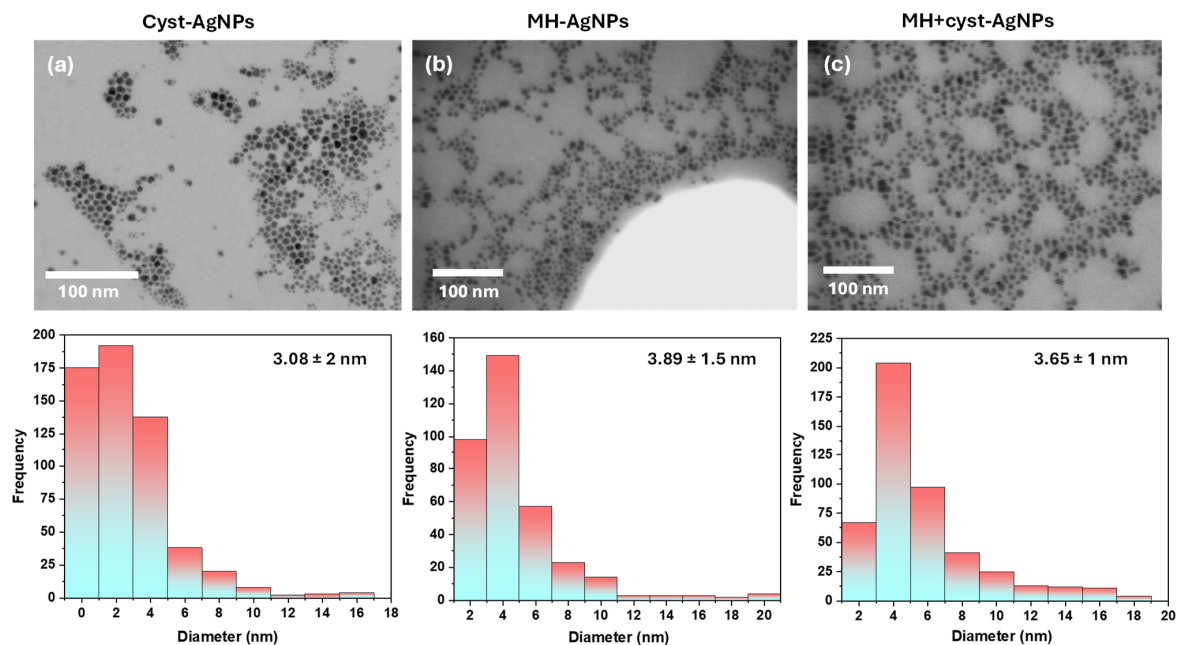
Figure 3. Showing the scanning electron microscopy (SEM) images of silver nanoparticles (**a**) Cyst-AgNPs, (**b**) MH-AgNPs, and (**c**) MH+cyst-AgNPs. Below is a respective histogram of the nanoparticles displaying the size distribution and mean diameter of the synthesized nanoparticles.

3.5. Elemental Analysis by EDX Spectroscopy

The EDX analysis offers valuable information about the elemental composition of the synthesized nanoparticles. The EDX spectrum shown in Figure 4a–c prominently displays a signal indicating the presence of silver (Ag) atoms. Additionally, there are strong peaks for carbon (C) and oxygen (O), suggesting a substantial layer of cysteamine (a), mercaptohexanol (b) and bifunctional MH+cyst-AgNPs (c) on the surface of the silver nanoparticles. The absorption peak at around 3 keV is characteristic of silver nanocrystals, aligning with findings reported by Ravichandran et al. [39]. Tables 1 and 2 present the weight percentages and atomic weight percentages of the silver nanoparticles, respectively. The EDX analysis showing silver (Ag) is the predominant element in all samples, with its atomic weight percentage decreasing from Cyst-AgNPs (54.23%) to MH-AgNPs (46.71%) and further to MH+cyst-AgNPs (45.26%). This trend suggests that the longer carbon chains of the capping molecules may hinder the detection of silver. The data in Table 2 reveal a higher carbon ratio compare to silver that increases with the extent of capping, demonstrating the successful functionalization of the silver nanoparticles.
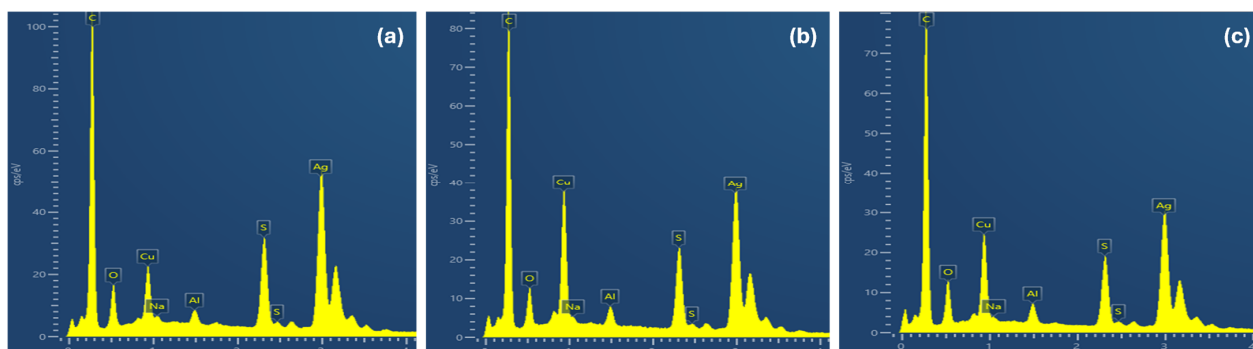
Figure 4. The energy-dispersive spectroscopy (EDS) showing a comprehensive analysis of the elemental composition of three types of silver nanoparticles: (**a**) Cyst-AgNPs, (**b**) MH-AgNPs, and (**c**) MH+cyst-AgNPs.

Table 1. Representing the weight percentages of the prime elements detected in the samples, primarily silver (Ag) and sulfur (S), for Cyst-AgNPs, MH-AgNPs, and MH+cyst-AgNPs. Each sample was measured at various points to ensure accuracy and representativeness of the data.

Element (Weight %)	C	O	Na	Al	S	Cu	Ag
Cyst-AgNPs	25.11	5.20	0.35	0.81	7.08	7.23	**54.23**
MH-AgNPs	25.88	4.25	0.28	1.07	6.24	15.56	**46.71**
MH+cyst-AgNPs	29.02	5.85	0.23	1.27	6.27	12.10	**45.26**

Table 2. Representing the atomic weight percentages of the main elements detected in the samples, primarily silver (Ag) and sulfur (S), for Cyst-AgNPs, MH-AgNPs, and MH+cyst-AgNPs. Each sample was measured at various points to ensure accuracy and representativeness of the data.

Element (Atomic %)	C	O	Na	Al	S	Cu	Ag
Cyst-AgNPs	63.39	9.85	0.46	0.91	6.69	3.45	**15.24**
MH-AgNPs	64.43	7.93	0.37	1.18	5.82	7.32	**12.96**
MH+cyst-AgNPs	66.30	10.03	0.27	1.29	5.37	5.23	**11.51**

3.6. DLS Analysis

The DLS spectroscopy of Cyst-AgNPs shows the overall hydrodynamic diameter at around 10 nm with a polydispersity index (PDI) of 0.62 (Figure 5, red) suggesting successful capping of amine functionality on the surface of silver nanoparticles. Without proper surface functionalization, AgNPs are prone to aggregation or reversion to silver ions; however, such behavior was not observed in our case. The presence of the capping agent, as inferred from the DLS data, supports the conclusion that the nanoparticles are well-stabilized. In contrast, the MH-AgNPs (Figure 5, blue) showed a slightly higher or similar hydrodynamic diameter at around 15 nm with a PDI of 0.4; the slight increase in the hydrodynamic diameter is possibly due to the longer carbon chain of 6-mercaptohexanol compared to that of cysteamine which could lead to greater steric hindrance and thus a larger effective size. On contrary the DLS spectra of MH+cyst-AgNPs showed a high hydrodynamic diameter of 44 nm with a PDI of 0.52 compared to cyst and MH-AgNPs. The hydrodynamic diameter measurement of nanoparticles can be influenced by several factors, including surface functionalization, solvent interaction, and particle aggregation. The dual functionality of MH+cyst-AgNPs might be creating a more complex surface layer that leads to a thicker and more hydrated surface coating, resulting in increasing the overall hydrodynamic diameter. Moreover, both mercaptohexanol and cysteamine have hydrophilic groups ($-OH$ and $-NH_2$, respectively), which attracts more water molecules, forming a larger hydration shell around each nanoparticle. Another factor is intermolecular interactions; the dual functionalization might lead to increased intermolecular interactions, such as hydrogen bonding or van der Waals forces, between the nanoparticles, which may promote slight aggregation or clustering in the solution, resulting in a higher apparent hydrodynamic diameter. In addition, the presence of two different functional groups might introduce steric hindrance, preventing the nanoparticles from coming too close to each other. This can stabilize the particles against aggregation to some extent but also contribute to an increased effective diameter. Overall, the DLS data validate the successful surface functionalization of silver nanoparticles.
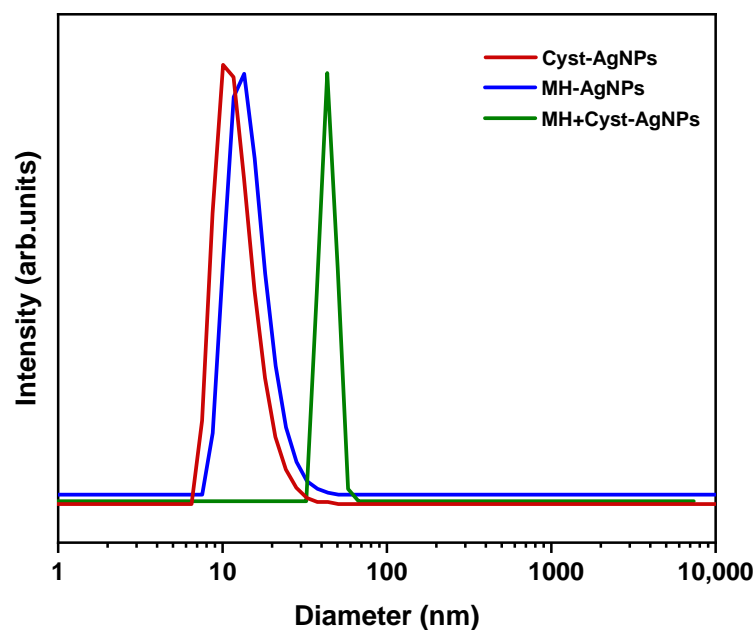
Figure 5. Displays the dynamic light scattering (DLS) spectra for three types of silver nanoparticles: Cyst-AgNPs (red), MH-AgNPs (blue), and MH+cyst-AgNPs (green) when dispersed in water. The spectra provide insights into the size distribution and stability of the nanoparticles in an aqueous environment.

3.7. Zeta Potential and Surface Charge

The zeta potential of nanoparticles is crucial for understanding and controlling their stability, surface properties, interactions with biological systems, and overall functionality in applications such as drug delivery, diagnostics, and material science. Colloidal stability and surface charge play key roles in how nanoparticles interact with cell membranes. Positively charged nanoparticles tend to have higher cellular uptake but may also exhibit greater toxicity, whereas negatively charged or neutral nanoparticles may have different biodistribution and clearance profiles. Additionally, the surface charge affects protein corona formation, which can alter nanoparticle functionality and biological response.

In this context, the zeta potential of silver nanoparticles was evaluated in acidic, neutral, and alkaline pH, as shown in Figure 6. The zeta potential of Cyst-AgNPs at neutral pH (7) was +21.56 mV. In an acidic environment, the amine groups ($-NH_2$) are likely to be protonated (NH_3+), resulting in a positive zeta potential of +28.37 mV. This positive charge suggests a tendency for non-specific protein adsorption, which can lead to the formation of a protein corona. In contrast, at higher (alkaline) pH, the amine groups become deprotonated, leading to a negative zeta potential of -10.56 mV. These zeta values indicate good colloidal stability for Cyst-AgNPs. This transition suggests that Cyst-AgNPs could exhibit improved stability at alkaline pH, reducing the likelihood of protein corona formation; however, the overall positive charge at neutral and acidic pH remains a concern for potential non-specific interactions in biological systems.

For MH-AgNPs, the zeta potential remains negative across acidic and alkaline pH, likely due to the ionization of $-OH$ groups on the nanoparticles surface. At acidic pH, the $-OH$ groups are less likely to be protonated, resulting in a neutral or negative zeta potential. In alkaline conditions, the deprotonation of the $-OH$ groups further reinforce a negative zeta potential. At neutral pH, MH-AgNPs exhibited a zeta potential of 9.44 mV, indicating partial deprotonation. While this suggests some level of stability, the negative charge may reduce non-specific protein adsorption compared to positively charged nanoparticles.
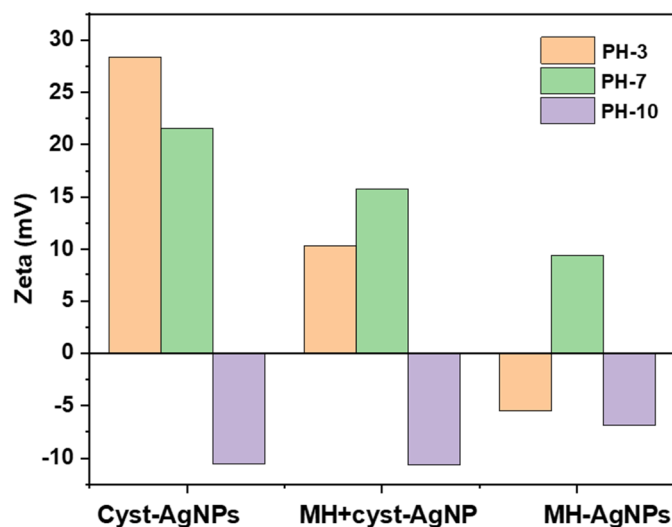
Figure 6. Illustrates the zeta potential of silver nanoparticles measured in water at three different pH levels: acidic (pH 3), neutral (pH 7), and alkaline (pH 10). The zeta potential values indicate the surface charge of the nanoparticles, which plays a critical role in their stability and interactions in biological systems.

The bifunctional cyst+MH-AgNPs followed a similar trend, with a positive zeta potential of +15.8 mV at neutral pH. At neutral pH, the positive charge from $-NH_2$ and the negative charge from $-OH$ groups balance each other, resulting in a neutral to slightly positive zeta potential. In acidic conditions, the $-NH_2$ groups are likely protonated, while the $-OH$ groups are not, leading to a slightly negative to neutral zeta potential. At higher pH, the deprotonation of $-OH$ groups result in a negative zeta potential of -6.86 mV. While these bifunctional nanoparticles exhibit good colloidal stability across pH levels, the presence of a positive charge at neutral pH raises concerns about non-specific protein adsorption and protein corona formation. This could significantly alter their behavior in biological environments, impacting their biodistribution, cellular uptake, and overall effectiveness.

3.8. Cell Viability Assay

The cell viability assay of silver nanoparticles (AgNPs) was conducted using normal breast epithelial cells (MCF10A) and two breast cancer cell lines (MDA-MB-231 and MCF-7) depicted in Figure 7. After 24 and 48 h of exposure, MH-AgNPs exhibited minimal toxicity across all cell lines, suggesting biocompatibility at concentrations up to 100 µg/mL. The slight decrease in viability observed in MCF-10A cells at concentrations above 40 µg/mL, followed by recovery at 48 h, indicates a transient stress response that normal cells can overcome.

In contrast, Cyst-AgNPs displayed significant cytotoxicity toward MCF-7 and MDA-MB-231 cancer cells, particularly at concentrations exceeding 40 µg/mL, while normal MCF10A cells were affected only at concentrations above 80 µg/mL. This suggests that Cyst-AgNPs may selectively target cancer cells at therapeutic doses, but caution is needed to minimize off-target effects in healthy tissue.

The bifunctional MH+Cyst-AgNPs demonstrated enhanced cytotoxicity at concentrations as low as 5 µg/mL. Interestingly, MDA-MB-231 cells exhibited some resistance at 24 h, maintaining 50% viability, but the prolonged exposure led to a sharp decrease at 48 h. The more pronounced effect on MCF-7 cells indicates that these nanoparticles may be especially effective against certain cancer subtypes. This differential response could be linked to differences in receptor expression, metabolic activity, or nanoparticle uptake between the two cancer cell lines.
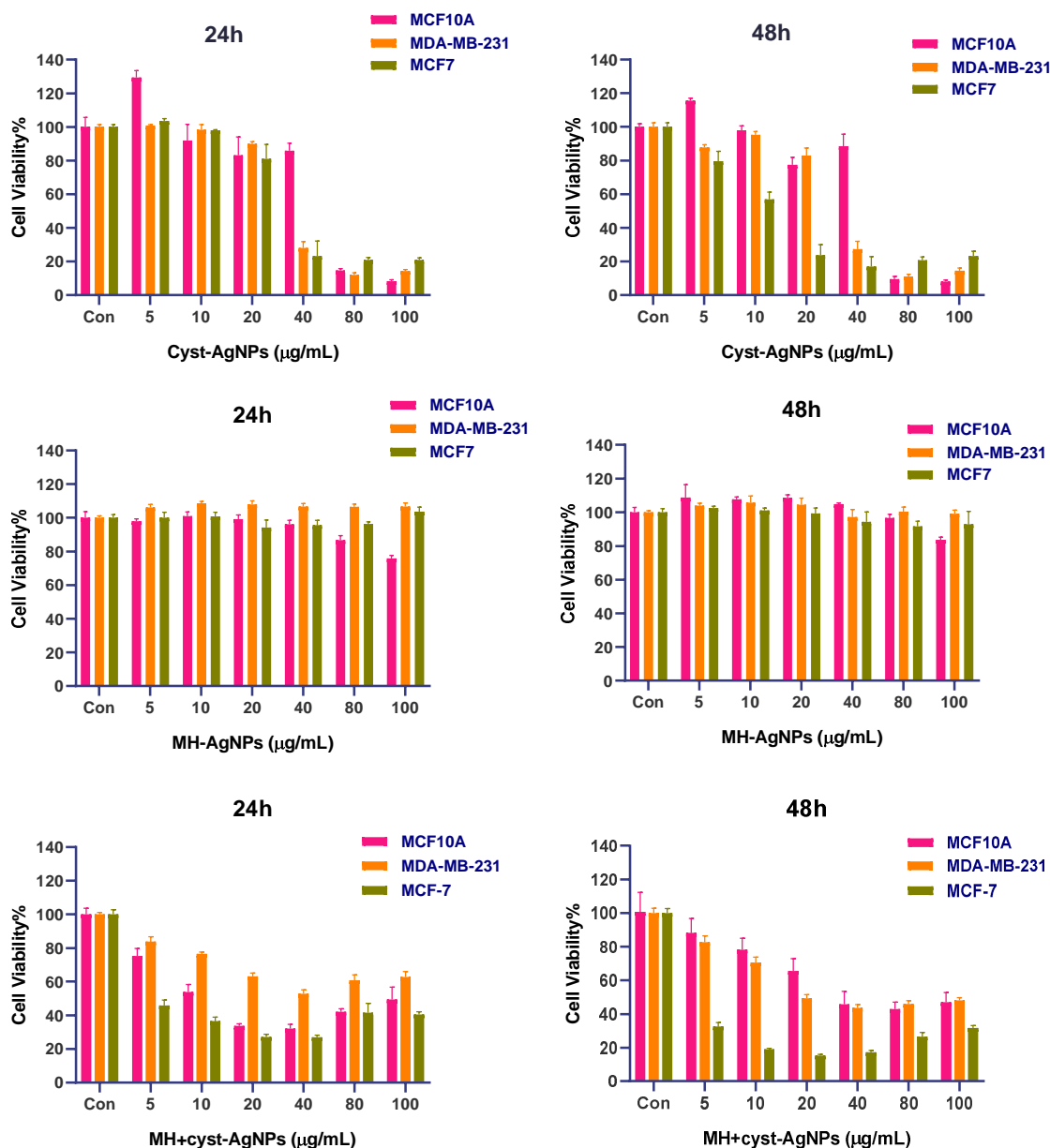
Figure 7. Presents the results of a cell viability assay evaluating the dose dependent toxicity effects of different silver nanoparticles on breast cancer cell lines MCF10A and MDA-MB-231, as well as normal breast cells (MCF-7). There are significant differences among all three cell lines, *p*-value < 0.001.

These findings underscore the potential of Cyst-AgNPs and bifunctional MH+Cyst-AgNPs as promising therapeutic agents, particularly for targeting aggressive cancers like triple-negative breast cancer (TNBC), which remains challenging to treat with conventional therapies. The significant cytotoxic effects of amine-functionalized AgNPs, particularly toward TNBC cells, highlight the need for further exploration of their mechanism of action.

One potential mechanism of cytotoxicity involves the generation of reactive oxygen species (ROS) by AgNPs, leading to oxidative stress, DNA damage, and eventual apoptosis in cancer cells. Additionally, the amine functional groups on the nanoparticles may enhance cellular uptake or disrupt cellular membranes, further contributing to their anti-cancer activity. Given the selectivity observed in the study, future research should focus on optimizing nanoparticle properties, such as size, surface charge, and coating materials, to maximize efficacy while minimizing harm to healthy cells.

Furthermore, in vivo studies are essential to assess the biodistribution, pharmacokinetics, and long-term safety of these nanoparticles. Understanding the interaction between AgNPs and the tumor microenvironment will also be critical in determining their potential as a clinical therapy. Finally, combination strategies with existing chemotherapeutics or radiotherapy could enhance treatment efficacy and reduce toxicity, offering a new avenue for cancer therapy.

4. Discussion

The silver nanoparticles were synthesized using a straightforward and well-known method, where silver nitrate was reduced by sodium borohydride, followed by functionalization with stabilizing agents such as cysteamine (Cyst-AgNPs), mercaptohexanol (MH-AgNPs), and a combination of both (MH+cyst-AgNPs). The synthesized nanoparticles were thoroughly characterized using UV–vis spectroscopy, FTIR, SEM, EDX, and DLS. The UV–vis spectra showed plasmon absorbance at 450 nm for Cyst-AgNPs, 500 nm for MH-AgNPs, and 475 nm for MH+cyst-AgNPs. The shift in SPR absorbance indicates the successful functionalization of the nanoparticles with the respective ligands [40].

SEM imaging confirmed that the nanoparticles ranged from 10 to 20 nm in size, consistent with DLS data. The larger hydrodynamic diameter observed for MH+cyst-AgNPs at 40 nm is likely due to the different surface charges, leading to a thick hydration layer and an increase in overall diameter [41]. Zeta potential measurements provided insights into the surface charge and stabilization of the nanoparticles across acidic, basic, and neutral pH levels. FTIR spectroscopy confirmed the successful surface functionalization of the silver nanoparticles, as indicated by the disappearance of the thiol peak at 2550 cm^{-1} [38].

The cell viability of silver nanoparticles was studied in both breast cancer and normal cell lines, including MCF-7, MDA-MB-231, and MCF10A. The assays indicated that MH-AgNPs did not induce toxicity in either cancerous or non-cancerous cell lines. In contrast, Cyst-AgNPs exhibited significant toxicity to both types of cells after 24 and 48 h of incubation. This difference in cellular response may be related to the surface charge of the nanoparticles [42]. MH-AgNPs possess a negative charge due to the presence of hydroxyl (−OH) groups, while cell membranes also carry a net negative charge from phospholipid head groups and various proteins. The resulting electrostatic repulsion may hinder the direct interaction and internalization of MH-AgNPs. Although negatively charged nanoparticles can still enter cells through endocytic pathways, this process tends to be slower and less efficient compared to the uptake of positively charged particles like Cyst-AgNPs, which carry amine (−NH$_2$) groups. The positive charge of Cyst-AgNPs facilitates their binding to the negatively charged cell membranes, leading to higher uptake and potential cellular disruption, including membrane integrity loss and apoptosis [43].

For MH+cyst-AgNPs, a significant reduction in cell viability was observed in MCF-7 cell lines, whereas only a moderate reduction was noted in MDA-MB-231 cells. These results suggest that the functionality and surface charge on nanoparticles are crucial factors in targeting cancer cells. The functionalization with both hydroxyl (−OH) and amine (−NH$_2$) groups might result in a net surface charge that does not strongly interact with the negatively charged cell membranes. This neutral or mixed charge could reduce the electrostatic attraction necessary for efficient nanoparticle uptake by the cells. The −OH groups on AgNPs may contribute to a more stable and less reactive nanoparticle surface, potentially lowering the ability of MH-cyst-AgNPs to generate reactive oxygen species (ROS) within cells—a critical pathway for inducing cytotoxicity and apoptosis. Another possibility is that the surface chemistry of MH-cyst-AgNPs might not favor the activation of specific endocytic pathways necessary for efficient internalization. If the nanoparticles do not effectively engage with receptors or other membrane components, their internalization could be impeded, reducing their cytotoxic potential. Consequently, MH-cyst-AgNPs may be less effective at inducing cell death in triple-negative breast cancer (TNBC) cells. The underlying mechanisms for these observations are not fully understood and require further investigation. In contrast, positively charged Cyst-AgNPs can facilitate electrostatic

interactions with the negatively charged cell membrane, enhancing the uptake of Cyst-AgNPs by TNBC cells [43]. Once inside the cells, Cyst-AgNPs can catalyze the production of ROS, which induces oxidative stress. Elevated ROS levels can damage cellular components such as DNA, proteins, and lipids, leading to apoptosis or necrosis [44]. Furthermore, once Cyst-AgNPs accumulate in the mitochondria, they can disrupt the electron transport chain, impair ATP production, and induce mitochondrial dysfunction. This disruption can trigger the release of pro-apoptotic factors, further promoting apoptosis [45].

The interaction of Cyst-AgNPs with cell membranes may also compromise membrane integrity. This disruption can lead to cell lysis or create pores that allow toxic molecules to enter the cell, exacerbating cytotoxic effects [46]. Additionally, silver ions released from Cyst-AgNPs can bind to thiol groups in proteins, altering their structure and function. This interference can disrupt critical cellular processes, including signal transduction, enzyme activity, and DNA repair mechanisms, ultimately leading to cell death [47]. The Cyst-AgNPs may activate apoptotic pathways by modulating the expression of pro- and anti-apoptotic proteins, activating caspases, or directly causing DNA fragmentation [45,48]. These mechanisms likely act synergistically, enhancing the overall cytotoxicity of Cyst-AgNPs towards MDA-MB-231 cells. Further experimental studies, including assays for ROS generation, mitochondrial membrane potential, caspase activity, and membrane integrity, are needed to confirm these mechanisms and fully understand the pathways involved.

5. Conclusions

In conclusion, we successfully synthesized bifunctional silver nanoparticles and thoroughly characterized them using various analytical techniques. We demonstrated that the choice of surface functionalization significantly impacts the cytotoxicity and cellular uptake of these nanoparticles, with distinct behaviors observed for each type of functionalization.

Specifically, our findings highlight the importance and potential of Cyst-AgNPs in targeting TNBC cells. Unlike other nanoparticle formulations, Cyst-AgNPs exhibited pronounced cytotoxic effects, particularly against MDA-MB-231 cells, a model for TNBC. This is significant given that TNBC lacks targeted therapies due to the absence of hormone receptors and HER2 expression, making it more challenging to treat with conventional methods.

The positive surface charge imparted by the amine groups on Cyst-AgNPs enhances electrostatic interactions with the negatively charged cell membranes of cancer cells, promoting efficient uptake and internalization. Once inside the cells, Cyst-AgNPs can induce the production of reactive oxygen species (ROS), leading to oxidative stress and triggering apoptosis. This mechanism underscores their potential as a therapeutic agent specifically designed to exploit the vulnerabilities of TNBC cells.

Our study demonstrates that amine-capped silver nanoparticles possess selective cytotoxicity against TNBC cells, offering a potential new avenue for treatment that exploits the unique surface charge interactions between nanoparticles and cancer cells. The detailed characterization of these nanoparticles provides a strong foundation for their further investigation as therapeutic agents. Future research should focus on understanding the detailed molecular pathways involved in their cytotoxicity, optimizing dosage and administration methods, and assessing their efficacy and safety in in vivo models. Additionally, exploring combinations with other therapeutic agents could enhance their effectiveness and provide new avenues for treating this aggressive form of breast cancer.

References

1. Bianchini, G.; Balko, J.M.; Mayer, I.A.; Sanders, M.E.; Gianni, L. Triple-negative breast cancer: Challenges and opportunities of a heterogeneous disease. *Nat. Rev. Clin. Oncol.* **2016**, *13*, 674–690. [CrossRef] [PubMed]
2. Won, K.A.; Spruck, C. Triple-negative breast cancer therapy: Current and future perspectives (review). *Int. J. Oncol.* **2020**, *57*, 1245–1261. [CrossRef] [PubMed]
3. Dai, X.; Li, T.; Bai, Z.; Yang, Y.; Liu, X.; Zhan, J.; Shi, B. Breast cancer intrinsic subtype classification, clinical use and future trends. *Am. J. Cancer Res.* **2015**, *5*, 2929–2943. [PubMed]
4. Caswell-Jin, J.L.; Plevritis, S.K.; Tian, L.; Cadham, C.J.; Xu, C.; Stout, N.K.; Sledge, G.W.; Mandelblatt, J.S.; Kurian, A.W. Change in survival in metastatic breast cancer with treatment advances: Meta-analysis and systematic review. *JNCI Cancer Spectr.* **2018**, *2*, pky062. [CrossRef]
5. Plevritis, S.K.; Munoz, D.; Kurian, A.W.; Stout, N.K.; Alagoz, O.; Near, A.M.; Lee, S.J.; van den Broek, J.J.; Huang, X.; Schechter, C.B.; et al. Association of screening and treatment with breast cancer mortality by molecular subtype in us women, 2000–2012. *JAMA* **2018**, *319*, 154–164. [CrossRef]
6. Bazak, R.; Houri, M.; Achy, S.E.; Hussein, W.; Refaat, T. Passive targeting of nanoparticles to cancer: A comprehensive review of the literature. *Mol. Clin. Oncol.* **2014**, *2*, 904–908. [CrossRef]
7. Blanco, E.; Shen, H.; Ferrari, M. Principles of nanoparticle design for overcoming biological barriers to drug delivery. *Nat. Biotechnol.* **2015**, *33*, 941–951. [CrossRef]
8. Arvizo, R.R.; Saha, S.; Wang, E.; Robertson, J.D.; Bhattacharya, R.; Mukherjee, P. Inhibition of tumor growth and metastasis by a self-therapeutic nanoparticle. *Proc. Natl. Acad. Sci. USA* **2013**, *110*, 6700–6705. [CrossRef]
9. Liu, Y.; Chen, C.; Qian, P.; Lu, X.; Sun, B.; Zhang, X.; Wang, L.; Gao, X.; Li, H.; Chen, Z.; et al. Gd-metallofullerenol nanomaterial as non-toxic breast cancer stem cell-specific inhibitor. *Nat. Commun.* **2015**, *6*, 5988. [CrossRef]
10. Soenen, S.J.; Demeester, J.; De Smedt, S.C.; Braeckmans, K. Turning a frown upside down: Exploiting nanoparticle toxicity for anticancer therapy. *Nano Today* **2013**, *8*, 121–125. [CrossRef]
11. Swanner, J.; Mims, J.; Carroll, D.L.; Akman, S.A.; Furdui, C.M.; Torti, S.V.; Singh, R.N. Differential cytotoxic and radiosensitizing effects of silver nanoparticles on triple-negative breast cancer and non-triple-negative breast cells. *Int. J. Nanomed.* **2015**, *10*, 3937–3953. [CrossRef]
12. Zanganeh, S.; Hutter, G.; Spitler, R.; Lenkov, O.; Mahmoudi, M.; Shaw, A.; Pajarinen, J.S.; Nejadnik, H.; Goodman, S.; Moseley, M.; et al. Iron oxide nanoparticles inhibit tumour growth by inducing pro-inflammatory macrophage polarization in tumour tissues. *Nat. Nanotechnol.* **2016**, *11*, 986–994. [CrossRef] [PubMed]
13. Yang, Y.; Zheng, X.; Chen, L.; Gong, X.; Yang, H.; Duan, X.; Zhu, Y. Multifunctional gold nanoparticles in cancer diagnosis and treatment. *Int. J. Nanomed.* **2022**, *17*, 2041–2067. [CrossRef] [PubMed]
14. Farzin, A.; Etesami, S.A.; Quint, J.; Memic, A.; Tamayol, A. Magnetic nanoparticles in cancer therapy and diagnosis. *Adv. Healthc. Mater.* **2020**, *9*, e1901058. [CrossRef]
15. Rezaei, B.; Yari, P.; Sanders, S.M.; Wang, H.; Chugh, V.K.; Liang, S.; Mostufa, S.; Xu, K.; Wang, J.-P.; Gómez-Pastora, J.; et al. Magnetic nanoparticles: A review on synthesis, characterization, functionalization, and biomedical applications. *Small* **2024**, *20*, 2304848. [CrossRef]
16. Wagner, A.M.; Knipe, J.M.; Orive, G.; Peppas, N.A. Quantum dots in biomedical applications. *Acta Biomater.* **2019**, *94*, 44–63. [CrossRef]
17. Hamidu, A.; Pitt, W.G.; Husseini, G.A. Recent breakthroughs in using quantum dots for cancer imaging and drug delivery purposes. *Nanomaterials* **2023**, *13*, 2566. [CrossRef]
18. Behi, M.; Gholami, L.; Naficy, S.; Palomba, S.; Dehghani, F. Carbon dots: A novel platform for biomedical applications. *Nanoscale Adv.* **2022**, *4*, 353–376. [CrossRef]
19. Tan, N.K.; Chan, H.; Lu, Z.; Zreiqat, H.; Lakhwani, G.; Lesani, P.; New, E.J. Ultrasensitive dual fluorophore-conjugated carbon dots for intracellular pH sensing in 3D tumor models. *ACS Appl. Mater. Interfaces* **2024**, *16*, 47303–47313. [CrossRef]
20. Ge, L.; Li, Q.; Wang, M.; Ouyang, J.; Li, X.; Xing, M.M. Nanosilver particles in medical applications: Synthesis, performance, and toxicity. *Int. J. Nanomed.* **2014**, *9*, 2399–2407. [CrossRef]
21. Murphy, M.; Ting, K.; Zhang, X.; Soo, C.; Zheng, Z. Current development of silver nanoparticle preparation, investigation, and application in the field of medicine. *J. Nanomater.* **2015**, *2015*, 696918. [CrossRef]

22. Wei, L.; Lu, J.; Xu, H.; Patel, A.; Chen, Z.-S.; Chen, G. Silver nanoparticles: Synthesis, properties, and therapeutic applications. *Drug Discov. Today* **2015**, *20*, 595–601. [CrossRef] [PubMed]

23. Liu, J.; Zhao, Y.; Guo, Q.; Wang, Z.; Wang, H.-Y.; Yang, Y.; Huang, Y. TAT-modified nanosilver for combating multidrug-resistant cancer. *Biomaterials* **2012**, *33*, 6155–6161. [CrossRef] [PubMed]

24. Fahrenholtz, C.D.; Swanner, J.; Ramirez-Perez, M.; Singh, R.N. Heterogeneous responses of ovarian cancer cells to silver nanoparticles as a single agent and in combination with cisplatin. *J. Nanomater.* **2017**, *2017*, 5107485. [CrossRef] [PubMed]

25. Liu, P.; Huang, Z.; Chen, Z.; Xu, R.; Wu, H.; Zang, F.; Wang, C.; Gu, N. Silver nanoparticles: A novel radiation sensitizer for glioma? *Nanoscale* **2013**, *5*, 11829–11836. [CrossRef]

26. Locatelli, E.; Naddaka, M.; Uboldi, C.; Loudos, G.; Fragogeorgi, E.; Molinari, V.; Pucci, A.; Tsotakos, T.; Psimadas, D.; Ponti, J.; et al. Targeted delivery of silver nanoparticles and alisertib: In vitro and in vivo synergistic effect against glioblastoma. *Nanomedicine* **2014**, *9*, 839–849. [CrossRef]

27. Sharma, S.; Chockalingam, S.; Sanpui, P.; Chattopadhyay, A.; Ghosh, S.S. Silver nanoparticles impregnated alginate-chitosan-blended nanocarrier induces apoptosis in human glioblastoma cells. *Adv. Healthc. Mater.* **2014**, *3*, 106–114. [CrossRef]

28. Miura, N.; Shinohara, Y. Cytotoxic effect and apoptosis induction by silver nanoparticles in HeLa cells. *Biochem. Biophys. Res. Commun.* **2009**, *390*, 733–737. [CrossRef]

29. Kawata, K.; Osawa, M.; Okabe, S. In vitro toxicity of silver nanoparticles at noncytotoxic doses to hepg2 human hepatoma cells. *Environ. Sci. Technol.* **2009**, *43*, 6046–6051. [CrossRef]

30. Antony, J.J.; Sithika, M.A.; Joseph, T.A.; Suriyakalaa, U.; Sankarganesh, A.; Siva, D.; Kalaiselvi, S.; Achiraman, S. In vivo antitumor activity of biosynthesized silver nanoparticles using Ficus religiosa as a nanofactory in DAL induced mice model. *Colloids Surf. B Biointerfaces* **2013**, *108*, 185–190. [CrossRef]

31. Beer, C.; Foldbjerg, R.; Hayashi, Y.; Sutherland, D.S.; Autrup, H. Toxicity of silver nanoparticles—Nanoparticle or silver ion? *Toxicol. Lett.* **2012**, *208*, 286–292. [CrossRef] [PubMed]

32. Guo, D.; Zhao, Y.; Zhang, Y.; Wang, Q.; Huang, Z.; Ding, Q.; Guo, Z.; Zhou, X.; Zhu, L.; Gu, N. The cellular uptake and cytotoxic effect of silver nanoparticles on chronic myeloid leukemia cells. *J. Biomed. Nanotechnol.* **2014**, *10*, 669–678. [CrossRef] [PubMed]

33. Guo, D.; Zhu, L.; Huang, Z.; Zhou, H.; Ge, Y.; Ma, W.; Wu, J.; Zhang, X.; Zhou, X.; Zhang, Y.; et al. Anti-leukemia activity of PVP-coated silver nanoparticles via generation of reactive oxygen species and release of silver ions. *Biomaterials* **2013**, *34*, 7884–7894. [CrossRef] [PubMed]

34. Sanpui, P.; Chattopadhyay, A.; Ghosh, S.S. Induction of apoptosis in cancer cells at low silver nanoparticle concentrations using chitosan nanocarrier. *ACS Appl. Mater. Interfaces* **2011**, *3*, 218–228. [CrossRef]

35. Zielinska, E.; Zauszkiewicz-Pawlak, A.; Wojcik, M.; Inkielewicz-Stepniak, I. Silver nanoparticles of different sizes induce a mixed type of programmed cell death in human pancreatic ductal adenocarcinoma. *Oncotarget* **2018**, *9*, 4675–4697. [CrossRef]

36. Singh, J.; Moore, W.; Fattah, F.; Jiang, X.; Zheng, J.; Kurian, P.; Beg, M.S.; Khan, S.A. Activity and pharmacology of homemade silver nanoparticles in refractory metastatic head and neck squamous cell cancer. *Head Neck* **2019**, *41*, E11–E16. [CrossRef]

37. Lee, C.M. A review on the antimutagenic and anticancer effects of cysteamine. *Adv. Pharmacol. Pharm. Sci.* **2023**, *2023*, 2419444. [CrossRef]

38. Oliva, J.M.; Ríos de la Rosa, J.M.; Sayagués, M.J.; Sánchez-Alcázar, J.A.; Merkling, P.J.; Zaderenko, A.P. Solvent-assisted in situ synthesis of cysteamine-capped silver nanoparticles. *Adv. Nat. Sci. Nanosci. Nanotechnol.* **2018**, *9*, 015001. [CrossRef]

39. Ravichandran, V.; Vasanthi, S.; Shalini, S.; Shah, S.A.A.; Tripathy, M.; Paliwal, N. Green synthesis, characterization, antibacterial, antioxidant and photocatalytic activity of Parkia speciosa leaves extract mediated silver nanoparticles. *Results Phys.* **2019**, *15*, 102565. [CrossRef]

40. Daublytė, E.; Zdaniauskienė, A.; Talaikis, M.; Charkova, T. Synthesis and functionalization of silver nanoparticles for divalent metal ion detection using surface-enhanced Raman spectroscopy. *J. Nanopart. Res.* **2023**, *26*, 6. [CrossRef]

41. Dawadi, S.; Katuwal, S.; Gupta, A.; Lamichhane, U.; Thapa, R.; Jaisi, S.; Lamichhane, G.; Bhattarai, D.P.; Parajuli, N. Current research on silver nanoparticles: Synthesis, characterization, and applications. *J. Nanomater.* **2021**, *2021*, 6687290. [CrossRef]

42. Hühn, D.; Kantner, K.; Geidel, C.; Brandholt, S.; De Cock, I.; Soenen, S.J.H.; Rivera_Gil, P.; Montenegro, J.-M.; Braeckmans, K.; Müllen, K.; et al. Polymer-coated nanoparticles interacting with proteins and cells: Focusing on the sign of the net charge. *ACS Nano* **2013**, *7*, 3253–3263. [CrossRef] [PubMed]

43. Augustine, R.; Hasan, A.; Primavera, R.; Wilson, R.J.; Thakor, A.S.; Kevadiya, B.D. Cellular uptake and retention of nanoparticles: Insights on particle properties and interaction with cellular components. *Mater. Today Commun.* **2020**, *25*, 101692. [CrossRef]

44. Salama, B.; Alzahrani, K.J.; Alghamdi, K.S.; Al-Amer, O.; Hassan, K.E.; Elhefny, M.A.; Albarakati, A.J.A.; Alharthi, F.; Althagafi, H.A.; Al Sberi, H.; et al. Silver nanoparticles enhance oxidative stress, inflammation, and apoptosis in liver and kidney tissues: Potential protective role of thymoquinone. *Biol. Trace Elem. Res.* **2023**, *201*, 2942–2954. [CrossRef] [PubMed]

45. Xiong, H.; Nie, X.; Cao, W.; Zhu, J.; Chen, J.; Liu, R.; Li, Y. Investigation of mitochondria-dependent apoptosis pathway and lipid peroxidation level induced by biosynthesized silver nanoparticles: Caspase-3 activation, BAK1/BCLx regulation and malondialdehyde production. *Cancer Nanotechnol.* **2024**, *15*, 13. [CrossRef]

46. Nie, P.; Zhao, Y.; Xu, H. Synthesis, applications, toxicity and toxicity mechanisms of silver nanoparticles: A review. *Ecotoxicol. Environ. Saf.* **2023**, *253*, 114636. [CrossRef]

47. Rohde, M.M.; Snyder, C.M.; Sloop, J.; Solst, S.R.; Donati, G.L.; Spitz, D.R.; Furdui, C.M.; Singh, R. The mechanism of cell death induced by silver nanoparticles is distinct from silver cations. *Part. Fibre Toxicol.* **2021**, *18*, 37. [CrossRef]

48. Assar, D.H.; Mokhbatly, A.-A.A.; Ghazy, E.W.; Elbialy, Z.I.; Gaber, A.A.; Hassan, A.A.; Nabil, A.; Asa, S.A. Silver nanoparticles induced hepatoxicity via the apoptotic/antiapoptotic pathway with activation of TGFβ-1 and α-SMA triggered liver fibrosis in Sprague Dawley rats. *Environ. Sci. Pollut. Res.* **2022**, *29*, 80448–80465. [CrossRef]